Supporting Information

Light-Induced Degradation of Mixed-cation, Mixed-halide Perovskite: Observed Rates and Influence of Oxygen

*Spencer G. Cira, Wiley A. Dunlap-Shohl, , Yuhuan Meng, Preetham P. Sunkari, Jordi H. Folch, and Hugh W. Hillhouse**

Department of Chemical Engineering, Clean Energy Institute, University of Washington, Seattle WA 98195-1750, USA

* Corresponding Author: h2@uw.edu

1. Experimental Methods; Film and Device Characterization

1.1 Sample Preparation: $FA_{0.8}Cs_{0.2}Pb(I_{0.83}Br_{0.17})_3$ precursor inks were prepared by dissolving stoichiometric CsI (FISHER SCIENTIFIC, 99.998%), FAI (Greatcell Solar Materials, >99.99%), PbI_2 (TCI AMERICA, 99.99%, trace metals basis) and $PbBr_2$ (TCI AMERICA, >98.0%) at 1 M concentration in 1/1 vol/vol N-methyl-2-pyrrolidone (NMP)/dimethylformamide (DMF), then allowed to dissolve overnight at 25°C. Glass substrates (15mm square) were cleaned with a four-step procedure by sonicating for 10 minutes each in (1) Alconox and DI water, then (2) DI water, then (3) acetone, and finally (4) 2-propanol. Shortly before spin coating, the substrates were cleaned for 10 minutes in an air plasma. $FA_{0.8}Cs_{0.2}Pb(I_{0.83}Br_{0.17})_3$ thin films were fabricated via spin coating in a N_2-filled glovebox. Before spin coating, the precursor inks were filtered through a 0.2 μm PTFE filter. 50 μL of the filtered precursor ink was spin coated at 4000 rpm for 45 sec. With 15 seconds remaining in the spin cycle, an antisolvent wash of 0.6 ml of toluene was dripped onto the sample to induce crystallization. Upon completion of the 45 second spin cycle, the films were annealed on a ceramic hotplate at 120°C for 15 minutes. Films averaged ~280 nm in thickness as measured with a Bruker OM-DektakXT stylus profilometer. For degradation experiments in which diffusion length measurements are also taken, 80nm Au contact pads (separation of 0.01 cm) were deposited via thermal evaporation at a rate of 2 Å/s. The $FAPbI_3$ and $FA_{0.8}Cs_{0.2}PbI_3$ films (discussed in SI section 5) were fabricated in the same way as the $FA_{0.8}Cs_{0.2}Pb(I_{0.83}Br_{0.17})_3$ with the adjustment of precursor solution inks to match the desired film composition. Additionally, to achieve the black alpha phase of FAPbI3, these films were annealed at 180°C for 15 minutes as opposed to 120°C. This is necessary to crystallize the alpha phase for pure (undoped) $FAPbI_3$ films.

1.2 Perovskite Film Characterization: Scanning electron microscopy (SEM) micrographs were obtained using a FEI XL30 SEM (Fig. S1d) and a ThermoFisher Scientific Apreo SEM (Fig. 1d).Thin film X-ray diffraction (XRD) measurements were collected with a Bruker D8 Discover instrument equipped with a Pilatus 100K large area 2D detector and a Cu anode (wavelength 1.542 Å, Kα radiation). The X-ray beam size was defined with a 0.3 mm collimator. X-ray photoelectron spectroscopy (XPS) measurements were taken on a ThermoScientific ESCALAB 250 with a monochromatic Al x-ray source and a 500-micron spot size. The binding energy scales were referenced to the C 1s peak at 284.8 eV. Optical absorbance spectra were collected from a PerkinElmer Lambda 1050 UV/vis/NIR spectrometer with an integrating sphere in laboratory atmosphere. Absorbance was calculated from separate measurements of sample percent transmittance and sample percent reflectance. Absorptance was calculated as $A = 1 - T - R$. Absolute intensity confocal photoluminescence was collected as described previously.[1] PL spectra were obtained with a modified Horiba LabRAM HR-800 with 532 nm laser excitation and a 10x objective lens. The adjustable confocal hole was set to 800 μm, and a 150 gr/mm Czerny−Turner monochromator blazed at 500 nm was used. The photon detection rate was calibrated using a blackbody source (IR- 301, Infrared Systems Development) at 850, 950, and 1050 °C with a 10 μm pinhole (the calibration factor was averaged between the three temperatures to minimize error). To calculate 1 sun excitation flux, an Oriel optical power meter and Thorlabs beam profiler were used to set the photon flux equal to above bandgap photon flux of the AM1.5 GT solar spectrum for a 1.66 eV material. Note that we can simply integrate the AIPL spectra to get a value for total emitted photon flux. Dividing this value by in incident photon flux gives us the external photoluminescence quantum yield ($PLQY$). From the $PLQY$, we can calculate an estimate for the quasi-fermi level splitting ($QFLS_{act}$) using the Ross relation: $QFLS_{act} = QFLS_{SQ} + k_B T \ln(PLQY)$ where

$QFLS_{SQ}$ is the detailed balance limit QFLS for an absorber at a given bandgap.[2] The bandgap is set equal to the peak PL emission energy such that changes in material bandgap (although small) can be accounted for to give a better estimate of the true quasi-fermi level splitting in the material.

1.3 *In-situ* Optoelectronic Degradation Experiments: For these degradation experiments, we place the sample, prepared as described above (with Au contact pads), in a Linkam Scientific LTSE420-P environmental test chamber, outfitted with an electric heater, gas ports, electrical probes, and windows above and below the sample. The atmosphere was controlled by connecting cylinders of N2 (99.998%, 4.8 grade, Praxair) and dry air (0.0 grade "Extra Dry," Praxair via twin Omega FMA5400/5500 mass flow controllers to the gas port on the Linkam chamber, allowing the O_2 content to be varied while maintaining constant total gas flow set at 3.0 L/min. We use a calibrated 540 nm LED (Lumencor SpectraX Light Engine) as the light source in a metallurgical upright microscope (Olympus BX53M, equipped with a 100x Mitutoyo Plan Apo NIR HR objective lens), and adjust the input power based on the sample band gap to obtain the desired 1 sun equivalent flux of above-band gap photons under the AM1.5G spectrum. Because only a small region of the film surface is illuminated, thermal energy can dissipate laterally. Additionally, a constant flow of gas across the surface helps keep the illuminated area at the same temperature as the dark regions. Photoconductivity was measured by connecting Au contacts to a Keithley 2420 source meter and sourcing + or – 3V while measuring current. The polarity of the applied voltage is switched every measurement to prevent artifacts from ion migration and buildup over the duration of the experiment due to consistent applied voltage. Photoluminescence quantum yield (PLQY) measurements are obtained simultaneously under 10 sun equivalent excitation. All data collected is automated with a Python master control program that takes measurements every 5 minutes. This general procedure has been described previously.[3]

1.4 *In-situ* Metallic Lead Formation Rate Experiments: Bare samples (without contacts) were used for measurements of metallic lead *in-situ*. For a typical degradation experiment, we place the sample prepared as describe above in a Linkam Scientific LTSE420-P environmental test chamber, outfitted with an electric heater, gas ports, and windows above and below the sample to allow light transmission. The test chamber is placed on a computer controlled XY stage. The nitrogen atmosphere was maintained by connecting a N_2 gas cylinder (99.998%, 4.8 grade) and setting the flow rate to 3L/min. with an Omega FMA5400/5500 mass flow controller. For these measurements, we use an Olympus 5x objective lens to degrade the sample. Periodically (every 8 minutes), we switch off the degradation beam and collect a measurement of transmittance with a 1300 nm monochromatic light source. The transmittance is measured by short-circuit current measurements from a Thorlabs InGaAs photodiode (FGA10) placed underneath the sample. To account for differences in responsivity as diode temperature fluctuates over the course of a degradation experiment due to natural thermal fluctuation in the lab, we also collect a '100% transmittance' measurement off the sample by moving the XY stage briefly such that the 1300 nm light is focused directly onto the photodiode (not passing through the sample). In this way, we can account for small changes in diode responsivity from time point to time point. All data collected is automated with a Python master control program.

1.5 Photovoltaic device fabrication and characterization: For fabrication of ITO/Poly-TPD/ $FA_{0.8}Cs_{0.2}Pb(I_{0.83}Br_{0.17})/C_{60}$/BCP/Ag perovskite solar cells, ITO-coated glass substrates (1.5x1.5 cm, 15 Ω sq^{-1}, Yingkou Shangneng Photoelectric Material Co.) were sonicated in Alconox

detergent solution, deionized water, acetone, and isopropanol for 10 min each, rinsing in deionized water in between each step. After the the last sonication, the substrates were dried with pressurized nitrogen and plasma cleaned in argon for 10 minutes. The substrates were then transferred to a nitrogen-filled glovebox, where they were spin-coated with a solution of ~1g/ml Poly-TPD (Poly[*N*,*N*′-bis(4-butylphenyl) -*N*,*N*′-bis(phenyl)-benzidine], Sigma Aldrich, M_W >20,000 g/mol) in ethanol at 3000 rpm for one minute. The substrates were then annealed in the glovebox at 600 °C for 10 minutes to drive off excess solvent. After Poly-TPD deposition, a monolayer of PFN-P2 (Poly(9,9-bis(3'-(*N*,*N*-dimethyl)-*N*-ethylammoinium-propyl-2,7-fluorene)-alt-2,7-(9,9-dioctylfluorene))dibromide, Sigma-Aldrich) was deposited by dynamically spin-casting a precursor of ~0.5 mg/ml of PFN-P2 in methanol at 5,000 rpm. Residual solvent is allowed to evaporate for 30 minutes before proceeding to the next step. Next, a 1 M solution of perovskite precursor ink (see S1.1 above) dissolved in 1:1 v:v dimethyl formamide and and *N*-methyl-2-pyrrolidone was spin-cast onto the Poly-TPD-coated substrates at 4000 rpm for 45 s. 15 seconds prior to the end of the spin step, 700 µL of toluene (Sigma Aldrich, anhydrous grade) was dropped onto the substrate. The films were annealed on a hot plate at 120 °C for 15 min. After the perovskite deposition, the substrates were transferred to a separate glovebox with a thermal evaporator (Angstrom Engineering Nexdep). 40 nm of C_{60} (Lumtec), followed by 7 nm of bathocuproine (Sigma Aldrich, sublimed grade) were evaporated from tungsten boats at maximum deposition rates of 0.5 and 0.3 Å s^{-1}, respectively. The substrates were then placed beneath a shadow mask to deposit patterned Ag (Kurt Lesker, 99.99%) contacts at a maximum rate of 2 Å s^{-1}. Current voltage (*J-V*) curves of single-junction $FA_{0.8}Cs_{0.2}Pb(I_{0.83}Br_{0.17})_3$ devices were measured under simulated AM1.5 G solar illumination with 0.2 V/s sweep rate for forward and reverse sweeps. The light source is an Oriel VeraSol-2 AAA Solar Simulator. An OSI Optoelectronics UV-100DQ Si photodiode was used to set the lamp intensity to equal the integrated above-bandgap AM1.5GT photon flux for a 1.66 eV bandgap material. A mask area of ~0.0453 cm^2 was used.

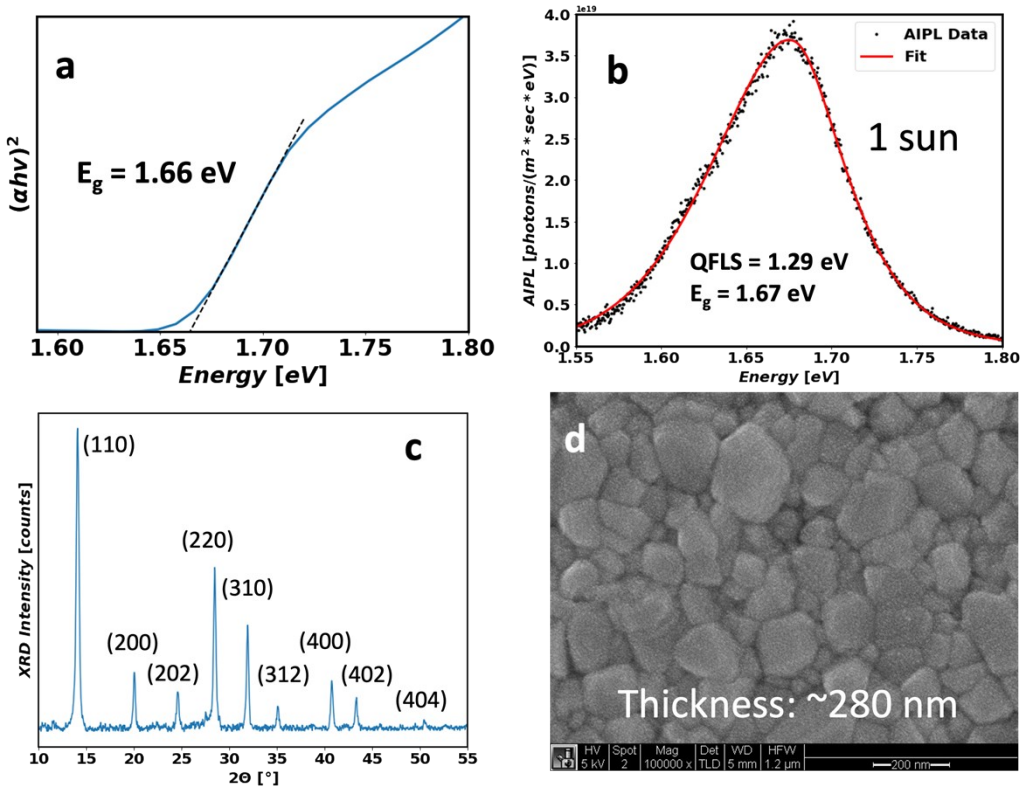

Figure S1. Characterization of $FA_{0.8}Cs_{0.2}Pb(I_{0.83}Br_{0.17})_3$ thin film. (a) Tauc plot with optical bandgap extrapolation, (b) absolute intensity photoluminescence (AIPL) spectra with full peak fit[4] to determine quasi-fermi level splitting (QFLS) under 1 sun equivalent photon flux, (c) x-ray diffraction pattern, and (d) scanning electron microscope image at 100kx magnification. QFLS under 1 sun equivalent illumination is equal to 93% of the radiative limit. The perovskite displays a strong absorption onset at the bandgap energy with clean morphology and diffraction pattern indicative of a single perovskite phase.

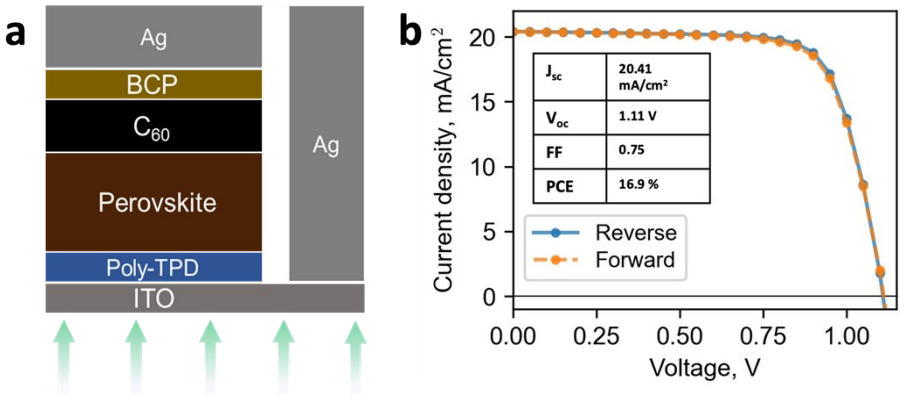

Figure S2. Device characterization of $FA_{0.8}Cs_{0.2}Pb(I_{0.83}Br_{0.17})_3$ devices. (a) Schematic of p-i-n device architecture, (b) current-voltage characteristic of the devices under 1 sun equivalent illumination. The devices made from the mixed cation, mixed halide films have good power conversion efficiency and an open-circuit voltage that is 81% of the radiative limit. Despite the films being thinner than desirable for high efficiency device fabrication, short-circuit current is still >86% of the radiative limit.

2. Light Sources Used for All Degradation Experiments

We aim to replicate conditions of normal solar illumination (Standard AM 1.5 Global Spectrum). To do so, we integrate the AM1.5 G spectrum above the bandgap of the perovskite to determine that the equivalent photon flux above the bandgap (1.66 eV) is 1.5×10^{21} photons/m^2/s. We perform calibration on each of the light sources as follows.

In-situ **Measurements**: All *in-situ* degradation measurements are taken on samples placed in an environmental control chamber in an upright microscope setup (Figure 3a provides a schematic of this setup). The incident beams are fed through via a liquid light guide cable from a Lumencor SpectraX Light Engine source. We use a Thorlabs Scanning Slit Optical Beam Profiler to assess the shape and distribution of the incident beam that is shown on the sample for each of the monochromatic LED emissions: red (~630 nm – red trace in Figure S3b), green (~540 nm – green trace in Figure S3b), and blue (~440 nm – blue trace in Figure S3b). We then assess the total power of the beam with an Oriel optical power meter. Homemade Python code is used to fit an appropriate distribution to the curves and determine the total equivalent photon flux (in units of photons/m^2/s) for the various LEDs and output settings. This procedure can be done for any objective lens to ensure proper calibration for both high magnification and low magnification lenses. The 1300 nm probe light is generated by a Thorlabs Fiber-Coupled LED (M1300F1-1300nm), and the emission spectrum is narrowed with a 1300 nm bandpass filter (Edmund Optics, 12nm FWHM).

Ex-situ **Measurements**: For *ex-situ* measurements, we illuminate perovskite samples in environmental control chambers with a broad-spectrum white LED that has emission between 400 and 700 nm (gold trace in Figure S3b). The resulting emission appears white to the eye. To ensure that the absorbed photon flux is close to that for those in the *in-situ* setup, we take single-junction perovskite solar cells (identical to those discussed in SI section 1) and determine the short circuit current under 1 sun equivalent illumination for the ~540 nm monochromatic LED in the microscope setup. We then take this identical device and place it under the broad-spectrum white LED and adjust the input power until identical short circuit current is reached. A standard silicon reference photodiode is used to ensure that the photon flux is the same for all *ex-situ* degradation experiments. In this way, we can achieve similar absorbed photon fluxes between the *in-situ* and *ex-situ* setups despite the varying spectral distributions of the light sources.

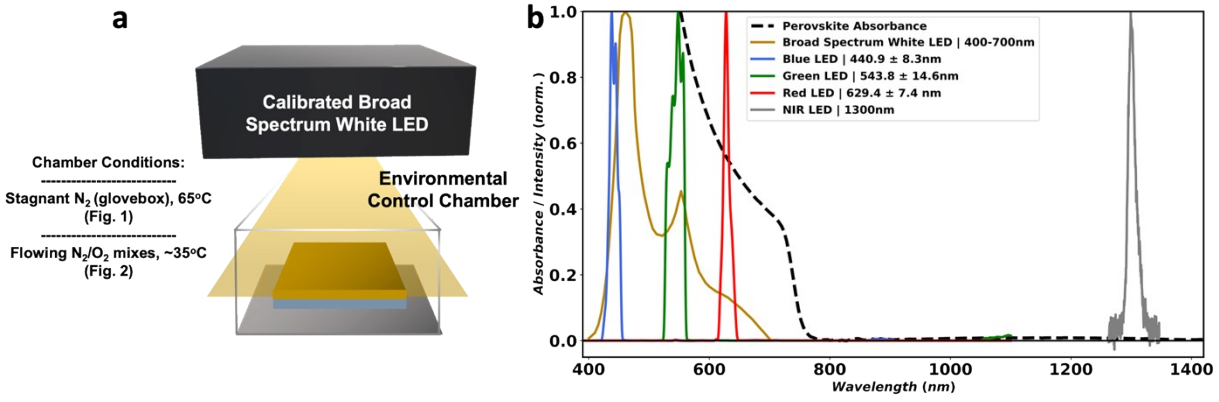

Figure S3. Light sources used for degradation. (a) Schematic of the *ex-situ* degradation setup. **(b)** Spectral distribution of LED light sources used for degradation (blue, green, red, and broad spectrum white) plotted with the $FA_{0.8}Cs_{0.2}Pb(I_{0.83}Br_{0.17})_3$ perovskite film absorbance and the 1300 nm near-infrared LED (used to probe Pb^0 formation but not used as a stressor). All degradation light sources are above the bandgap of the material while the 1300 nm probe beam is well below.

3. Identification of Degradation Products

Here, we present zoomed in diffractograms along with reference patterns for identification of the crystalline degradation products that form during LID. The information is shown below in Figure S4 and is identical that shown in Figure 1c. As discussed in the main text, the primary crystalline degradation product that we observe is metallic lead (Pb^0) which is identifiable by the (111) and (200) reflections at 31.3° and 36.3°, respectively. At later stages of degradation, we also observe the (001) reflection of cubic $FAPbBr_3$ at ~14.8° and the (001) reflection of PbI_2 at 12.6°. The former may be the result of I_2 loss which leaves behind a top layer of Br enriched perovskite while the latter may form from simultaneous I_2 loss and consumption of organic formamidinium. We also observe a peak shift of the main (110) reflection of $FA_{0.8}Cs_{0.2}Pb(_{0.83}Br_{0.17})_3$ at ~14.1° to lower angles suggesting that the lattice is expanding as the material decomposes.

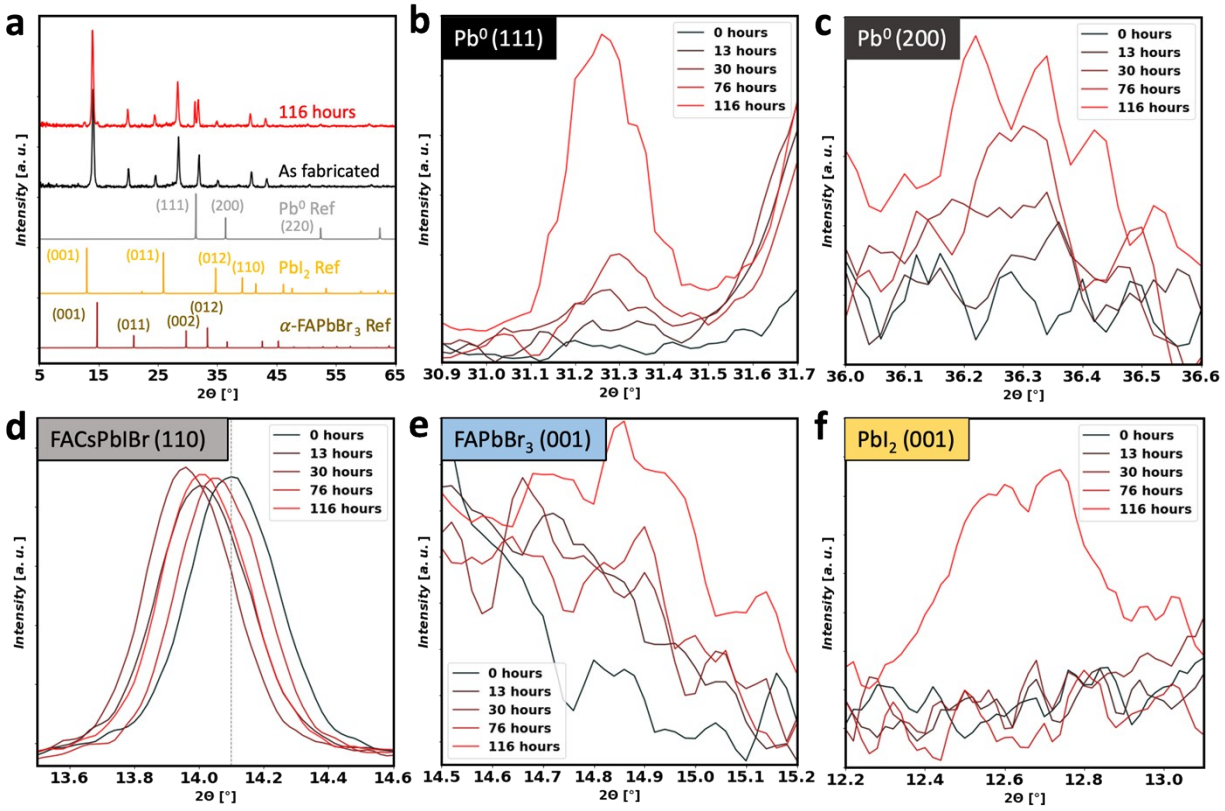

Figure S4. Identification of crystalline degradation products during LID at 65°C under 1 sun illumination. (a) Diffraction patterns of samples as fabricated and after 116 hours of photo stress (background subtracted) along with simulated reference patterns for relevant degradation products (reference patterns: Pb^0: COD #1011119, PbI2: COD #1010062, α-$FAPbBr_3$: COD #7130785). (b-f) Zoomed-in look at the region of the diffractogram associated with plane reflections for (b) Pb^0 (111), (c) Pb^0 (200), (d) $FA_{0.8}Cs_{0.2}Pb(_{0.83}Br_{0.17})_3$ (110), (e) $FAPbBr_3$ (001), and (f) PbI_2 (001).

To further probe the chemical makeup of the FACsPbIBr films before and after LID, we performed x-ray photoelectron spectroscopy (XPS) on fresh and degraded films. Figure S5 presents the high resolution Pb 4f spectra from these measurements. A low energy shoulder, indicative of metallic lead, that is not present

in the fresh film is observed in the degraded film. Voigt profile fits to the high resolution Pb 4f spectra indicate that only Pb^{2+} is present in the fresh film whereas both Pb^{2+} and Pb^{0} are present in the degraded film. The broadening of the Pb^{2+} peaks after degradation suggests the presence of lead atoms that are in intermediate oxidation states in addition to those in the pure 2+ and 0 state.[5]

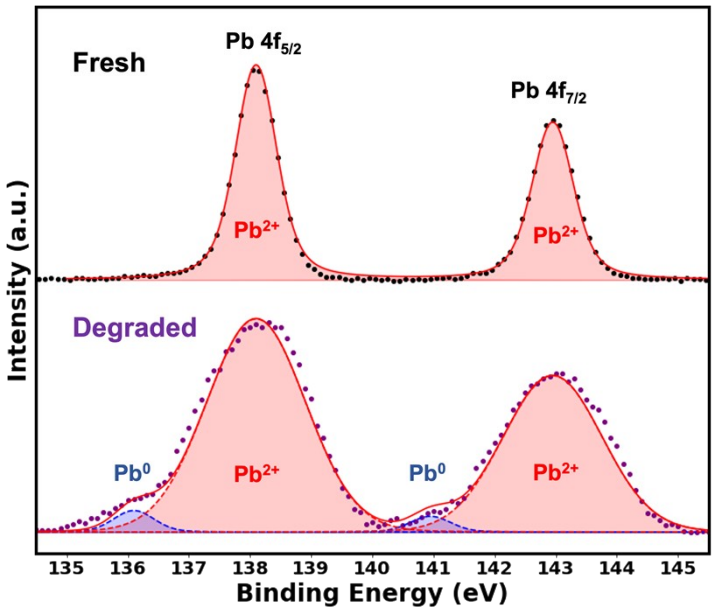

Figure S5. XPS measurements of fresh and degraded films. High resolution Pb 4f spectra for a fresh and degraded FACsPbIBr film. The degraded film was stressed at 145°C under 1 sun equivalent illumination for 5 hours.

4. Estimation of Initial Pb^0 Formation Rate Calculated from 1300 nm Transmittance

Internal optical absorbance A is defined in the following ways:

$$A = \log_{10}(e)\alpha l = -\log_{10}\left(\frac{T}{1-R}\right)$$

where α is the absorption coefficient at the measured wavelength, l is the path length of the absorbing medium (film thickness), T is the fractional transmittance of the film, and R is the fractional reflectance. Thus, internal absorbance measurements enable direct measurements of material thickness if the absorption coefficient is known. We can take the time derivative of absorbance $\left(\frac{dA}{dt}\right)$ to calculate a change in material thickness assuming that the absorbance change is solely indicative of a singular species generation or consumption. If UV-Vis-NIR measurements are done such that we can obtain both T and R at a given wavelength at various time points during a degradation experiment, then the absolute internal absorbance is directly obtainable. If we have multiple time points, then we can simply fit a line to a plot of absolute internal absorbance versus time to determine $\frac{dA}{dt}$. This result is true for any species so long as the absorbance change calculated is attributable to that species alone. However, in our *in-situ* degradation setup, we can only obtain transmittance measurements. The setup is advantageous in that we can obtain data with high time resolution that does not require us to remove samples from a given environment. To determine rates, we aim rather to determine the change in absorbance with the following equation:

$$\Delta A = -\log_{10}\left(\frac{T_{t=t}}{T_{t=0}}\right) - \log_{10}\left(\frac{1-R_{t=0}}{1-R_{t=t}}\right)$$

If changes in reflectance are small, then the second term in the above equation vanishes and we arrive at an expression that relates transmittance changes alone to change in absorbance:

$$\Delta A = -\log_{10}\left(\frac{T_{t=t}}{T_{t=0}}\right)$$

Dividing ΔA by the time interval ΔT during early degradation periods gives $\frac{dA}{dt}$. From this and as described in previous publications on the chemical reaction kinetics of perovskite semiconductors,[6,7] we can then quantify the rate of chemical reaction for an absorbing species *i* by the following equation:

$$r_i = \frac{\rho_i \cdot \log_e(10)}{M_i \cdot \alpha_i} \cdot \frac{dA}{dt}$$

where ρ_i is the density, M_i is the molecular weight, α_i is the absorption coefficient for the absorbing species i that is either being accumulated or depleted. $\frac{dA}{dt}$ is the rate of change of

internal absorbance, calculated during 'early-times' (over the first ~120-240 minutes of a degradation experiment).

A necessary step to quantifying r_{Pb^0} is to determine α_{Pb^0} (density and molecular weight of Pb^0 are readily known but absorption coefficient is reported less). To determine the absorption coefficient of Pb^0 across the visible and near-infrared, we deposited thin films (50 nm) of Pb^0 on glass slides and measured the internal absorbance by UV-Vis-NIR (determined from transmittance and reflectance spectra). See Figure S6 below for the absorption coefficient spectrum determined for 3 films. Variation is generally small, so we averaged the 3 spectra and used the average as our experimentally determined absorption coefficient for Pb^0.

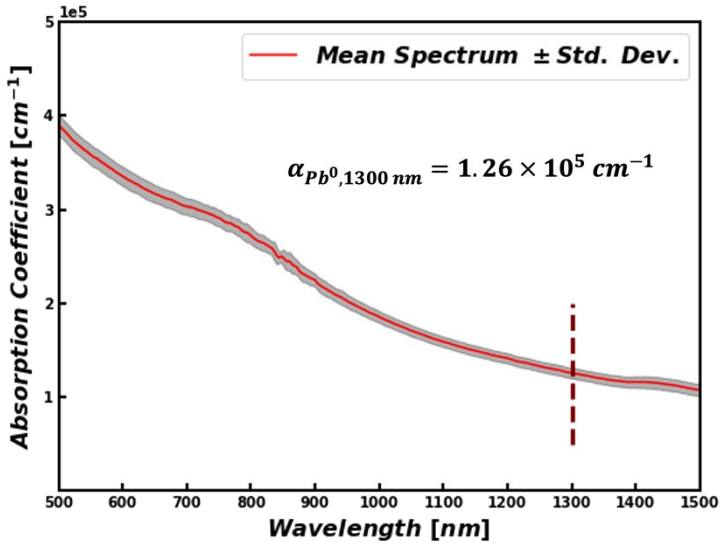

Figure S6. Determination of Pb^0 Absorption Coefficient at 1300 nm. UV-Vis-NIR absorbance measurement for metallic lead thin films (50 nm thickness). Thin films of lead were deposited by thermal evaporation on soda-lime glass substrates. Calibration of the tuning factor on the thermal evaporator was done by measuring film thicknesses with stylus profilometry. The absorption coefficient of metallic lead was determined to be 1.26 x 10^5 cm^{-1} at 1300 nm.

To determine the initial rate of lead formation *in-situ*, we focus on the sub perovskite bandgap (near-infrared) region of the electromagnetic spectrum for optical characterization. In this region, Pb^0 is the only species that will appreciably absorb light. Thus, sub bandgap absorbance changes indicate the formation of Pb^0 as the perovskite degrades during light-induced degradation. For accurate measurements, we need to select a wavelength that changes minimally in reflectance. To determine an appropriate wavelength, we obtained *ex-situ* UV-Vis-NIR measurements of transmittance, reflectance, and absorptance (calculated from $A = 1 - T - R$) over the course of LID at 1 sun photon flux from a white LED at 65°C in a N_2 filled glovebox. From these measurements, we determined that 1300 nm measurements were optimal for quantifying r_{Pb^0} *in-situ*. The results of this experiment are shown below in Figure S7.

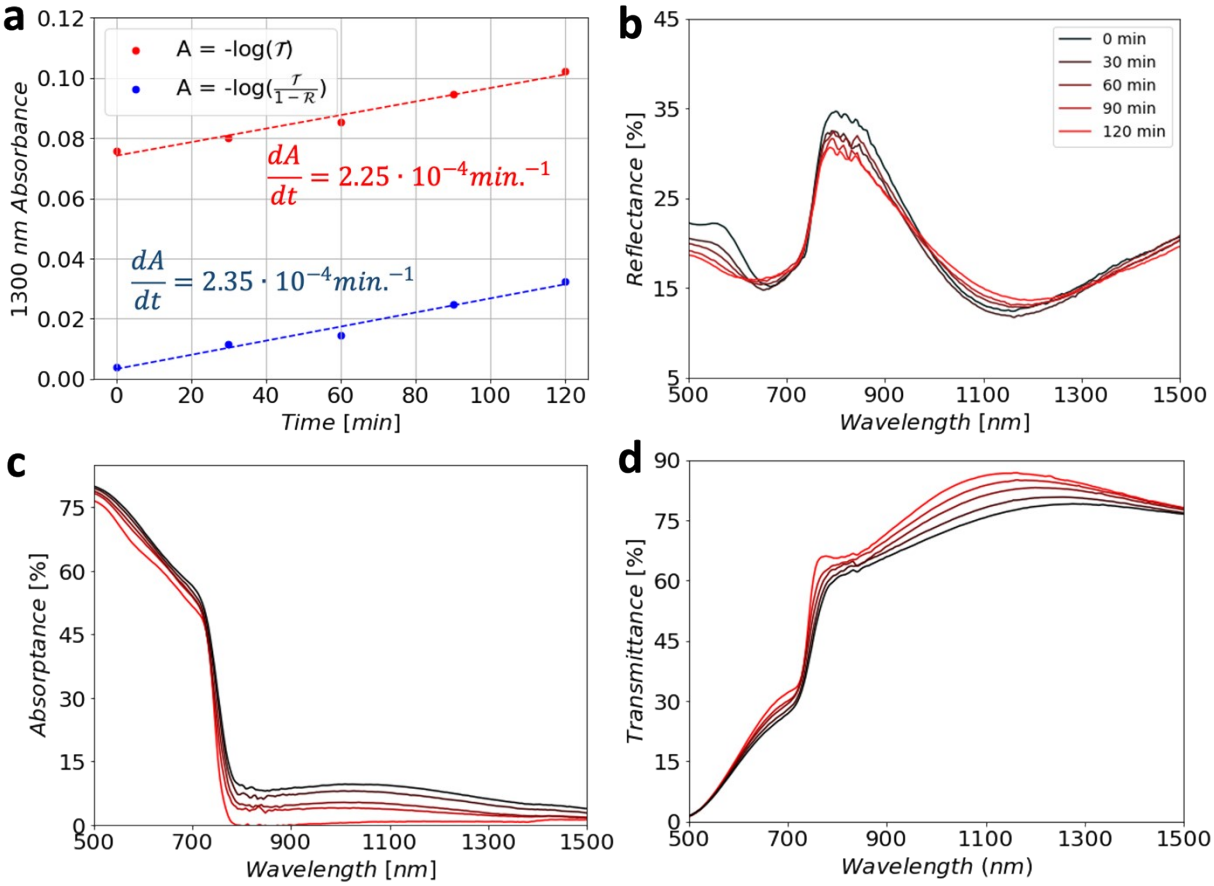

Figure S7. *Ex-situ* UV-Vis-NIR measurements to determine appropriate wavelength for Pb^0 detection with *in-situ* transmittance. (a) Absorbance at 1300 nm over time calculated from transmittance alone and with the effects of reflectance. Also included are (b) reflectance, (c) absorptance, and (d) transmittance spectra over the course of degradation. The conditions of this degradation experiment were 65°C under 1 sun equivalent illumination from a white LED (emission between 400nm and 700nm) in an N_2 filled glovebox. S5a shows that the reflectance changes are small during the early parts of degradation such that the rate of Pb^0 formation can be determined accurately from 1300 nm transmittance measurements alone. Percent error between the reflectance corrected and uncorrected fits is <5%.

5. Derivation of Rate Expression for Light-Induced Degradation Pathway

The plausible complete chemical reaction pathway with elementary steps for the light-induced decomposition of $FAPbI_3$ is shown below. Here, we assume that FA^+ and I^- are much more reactive than Cs^+ and Br^-, respectively, such that during early times we can consider only the reactions of FA^+, I^-, and Pb^{2+}. Thus, we have a rate expression that considers $FAPbI_3$ as the reacting perovskite species. The reaction yields the following net reaction of $FAPbI_3$ reacting with photons (via photoexcited electrons and holes) to produce Pb^0 and I_2 gas (FAI is assumed to be the volatile organic in this case):

$$FAPbI_3 + h\nu \rightarrow Pb^0 + I_2 + FAI \qquad \text{(LID)}$$

The reaction starts with photoexcitation and proceeds via oxidation of iodide interstitials:

$$h\nu \rightarrow e^- + h^+ \qquad \text{(1LID)}$$

$$FAPbI_3 \rightleftharpoons FAPbI_2^+ + I^- \qquad \text{(2LID)}$$

$$I^- + h^+ \rightarrow I^{\cdot} \qquad \textbf{(3LID)}$$

$$FAPbI_2^+ + e^- \rightarrow FAI + Pb^0 + I^{\cdot} \qquad \text{(4LID)}$$

$$2I^{\cdot} \rightarrow I_2 \qquad \text{(5LID)}$$

Now, we derive a mathematical form for r_{Pb^0} based on the proposed pathway. From this pathway, we begin with the following statement about r_{Pb^0}:

$$r_{Pb^0} = r_{4LID} = k_{4LID} a_{e^-} a_{FAPbI_2^+}$$

where a_{e^-} is the activity of electrons, $a_{FAPbI_2^+}$ is the activity of $FAPbI_2^+$ in the perovskite structure, and k_{4LID} is the temperature dependent rate constant for the forward reaction. We assume there to be a RDS (step 3LID) that (with note that we have 1:1 stoichiometry) allows us to write the following expression for r_{Pb^0}:

$$r_{Pb^0} = r_{3LID} = k_{3LID} a_{h^+} a_{I^-}$$

where a_{h^+} is the activity of holes, a_{I^-} is the activity of iodide defects in the perovskite structure, and k_{3LID} is the temperature dependent rate constant for the forward reaction. If we assume that the equilibrium kinetics of step 2LID are much faster than consumption of I^- in step 3LID, we come to the final mathematical expression for r_{Pb^0}:

$$r_{Pb^0} = k_{0,LID} exp\left(-\frac{E_{A,LID}^{eff}}{k_B T}\right) I_{in}^{n} \quad (1)$$

where $k_{0,LID}$ is the temperature independent prefactor, $E_{A,LID}^{eff}$ is the effective activation energy of the LID decomposition reaction, I_{in} is the incident above bandgap photon flux, and n is the effective order of the above bandgap photon flux.

Comments on assumptions for this degradation pathway

A primary assumption of the reaction pathway is related to the low electron affinity of Pb^{2+}. We assume that the rate of Pb^{2+} reduction to Pb^0 is determined by the loss of I_2 from the film. Effectively, Pb^{2+} (even in the presence of photoexcited conduction band electrons) is unlikely to be reduced. However, the relative ease of oxidation of halide species, followed by mass transport and removal from the film, creates an electrochemical driving force for electrons due to a charge imbalance that develops as holes are consumed. Here, we choose to consider only the 'early-time' periods of degradation such that the activity of all intrinsic material defects remains relatively constant. We also note that the final mathematical rate expression is identical to that which could be formulated by a simple empirical expression (with the assumption that perovskite activity is constant) from the net reaction equation.

Lastly, we mention the assumption that $FAPbI_3$ be considered the reactive perovskite unit where we ignore the small affects associated with Cs^+ and Br^-. To test this, we fabricated $FA_{0.8}Cs_{0.2}PbI_3$ (E_g~1.59 eV) and $FAPbI_3$ (E_g~1.51 eV) via the same methods as those use for the $FA_{0.8}Cs_{0.2}Pb(I_{0.83}Br_{0.17})_3$ films. To obtain the black α-phase of $FAPbI_3$, an anneal temperature of 180°C was used. All other steps in the fabrication procedures are the same as those described in SI section 1. We replicated the experimental conditions of Figure 1 in the main text (65°C, ~1 sun equivalent photon flux in a stagnant N_2 filled glovebox) to determine if LID proceeds in these compositions. We monitor the changes in the internal absorbance. Figure S8 shows the results of this experiment where we can clearly observe that the sub bandgap absorbance increases for both compositions after a 10-hour degradation period, suggesting that indeed Pb^0 is being formed during LID. It appears that the rate of sub-bandgap absorbance increase (and thus the rate of Pb^0 formation) appears to be slower in these compositions. The differences among the various FA-rich compositions will be the subject of future studies.

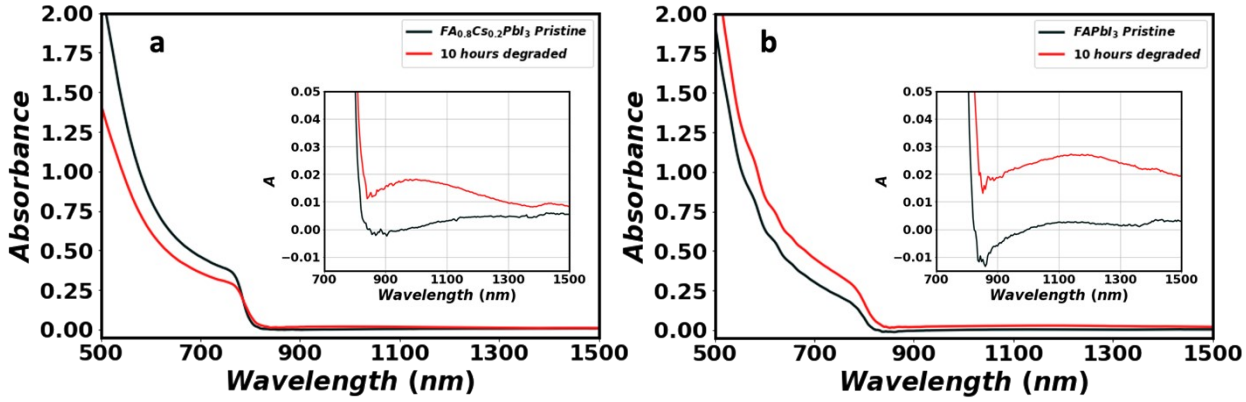

Figure S8. *Ex-situ* UV-Vis-NIR absorbance of $FA_{0.8}Cs_{0.2}PbI_3$ and $FAPbI_3$ during LID. Absorbance of (a) $FA_{0.8}Cs_{0.2}PbI_3$ and (b) $FAPbI_3$ films before (black trace) and after (red trace) a 10-hour period of light-induced degradation at 65°C in a N_2 glovebox. Insets are zoomed in regions from 700 to 1500 nm

6. Influence of Photon Flux on Photoactive Species Activity

To determine the influence of above bandgap photon flux on photoexcited species activity, we performed photon flux dependent photoconductivity measurements (see Figure 4c in the main text). The justification for assigning the value n to this rate constant is explained in full in our prior paper on $MAPbI_3$ degradation.[2] In brief, we can conclude that photoconductivity is directly proportional to the photoactivity species activity with the following discussion.

By combining equations for the definition of thermodynamic activity of a species and assuming quasi-thermal equilibrium of an intrinsic semiconductor, we can write the activity of photoexcited holes in the perovskite under illumination as the following:

$$a_{h+} = exp\left(\frac{-k_B T(\ln p_h - \ln N_v) + E_v - \mu_h^0}{k_B T}\right)$$

where p_h, N_v, E_v, and μ_h^0 are the hole concentration, effective density of states in the valence band, valence band energy level, and chemical potential of holes under some standard thermodynamic condition, respectively. From this, we can pull out all constants into one (C) and conclude that activity of holes (a_h) is directly proportional to hole concentration:

$$a_{h+} = C \cdot p_h$$

We also know that photoconductivity is directly proportional to concentrations of photoexcited species by the following equation:

$$\sigma_{ph} = q\,(\mu_h^{mob} p_h + \mu_e^{mob} n_e)$$

where q and n_e are the fundamental unit of electric charge and the electron concentration, respectively. μ_h^{mob} and μ_e^{mob} are the mobilities of holes and electrons, respectively (denoted as such so as not to confuse with chemical potential). For an intrinsic semiconductor under 1 sun illumination, the excited carrier populations should be much larger than the equilibrium populations, and thus $n_e \approx p_h$, so $\sigma_{ph} \approx q\left(\mu_h^{mob} + \mu_e^{mob}\right)p_h$. This allows us to conclude that photoconductivity is directly proportional to activity of holes.

Thus, the power law fit of photoconductivity versus photon flux should yield a parameter that accurately quantifies the incremental increase in photoexcited species activity with increases in above bandgap photon flux (photons that cannot be absorbed will obviously not influence photoexcited species activity). The absolute activity will be lumped into the pre-exponential factor of equation 1, $k_{0,LID}$. Again, note that this result matches experimental data of metallic lead rates quite well (figure 4d in the main text). The relationship between photoconductivity and incident

photon flux in solids has been discussed previously by Schellenberg and Kao.[8] They concluded that it should take on the following form:

$\sigma_{ph} \propto I^{\beta}$

where β typically takes a value between 0.5 and 1 ($0.5 \leq \beta \leq 1$) for solid semiconductors. Our result of 0.72 in Figure 4c agrees with this earlier theoretical result.

7. Explanation of Procedure for Data Fitting and Testing

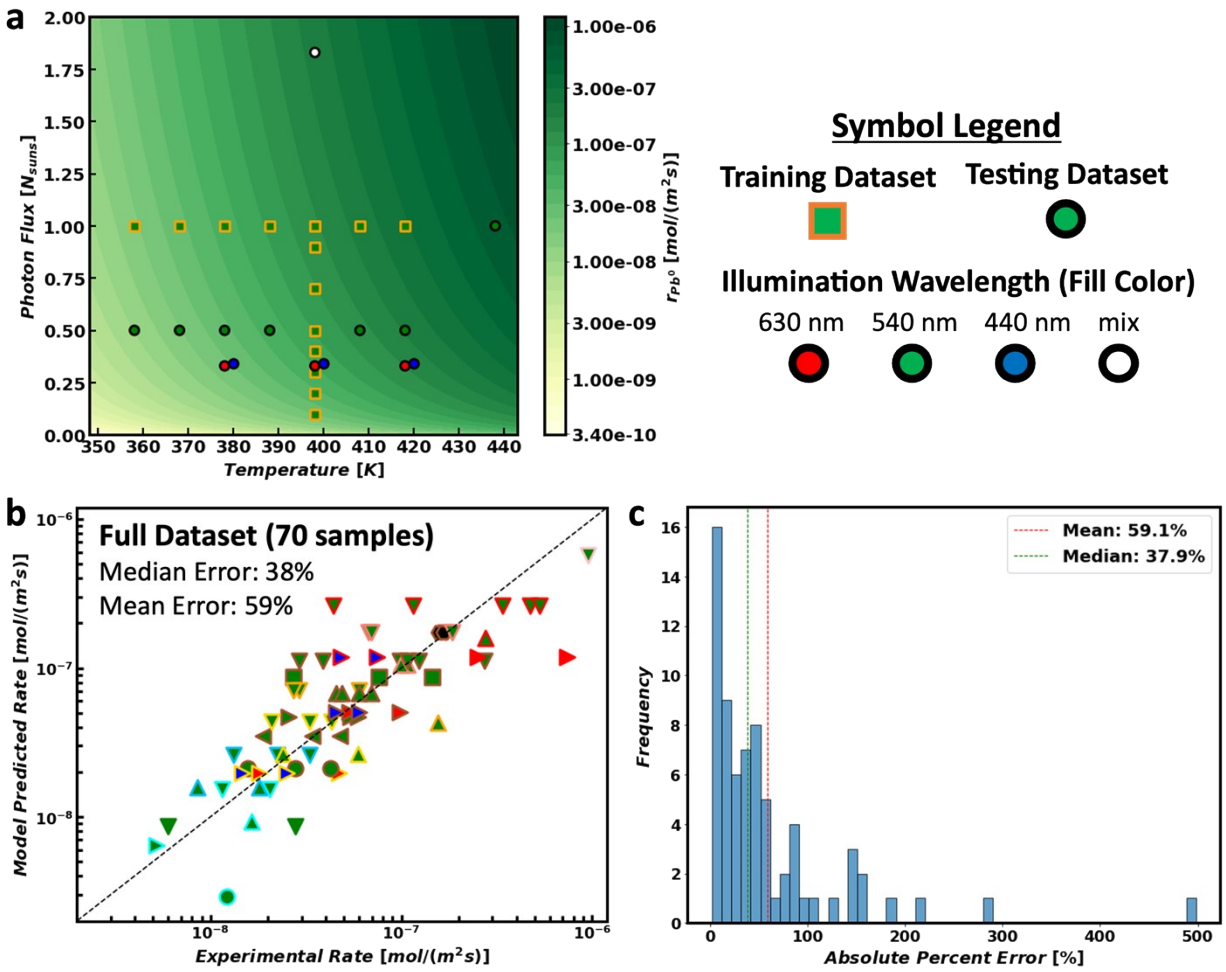

Figure S9. Explanation of complete LID dataset. (a) Contour plot of model predicted r_{Pb^0} over a range of temperatures and photon fluxes. On the contour plot are symbols that reference specific conditions associated with the training dataset and test dataset. The training dataset (orange squares) includes all runs degraded under 540 nm light that are at 1 sun *or* at 125°C (0.1-1 suns). The test dataset (black circles) includes 540 nm illumination runs at 0.5 suns over a range of temperatures (85, 95, 105, 115, 135, 145°C). It also includes 2 runs at 1.86 suns with a mixture of wavelengths (white filled), duplicates of runs at 0.33 suns and temperatures of 378, 398, and 418 K for 440 nm (blue filled) and 630 nm (red fill) illumination (these points are offset to be identifiable), and one run at 165°C, 1 sun to provide confidence in our hypothesis of Arrhenius behavior over a wide range of temperatures. (b) Parity plot for the complete dataset that consists of both training and test datasets combined (70 samples in total). (c) Histogram of the absolute percent error for the complete dataset.

To determine each parameter of the LID equation 1, we perform the following fitting procedures:

Activation Energy ($E_{A,LID}^{eff}$): The subset of the training dataset used for activation energy determination is runs at 1 sun, 540 nm light, over temperatures from 85-145°C. From the averages of r_{Pb^0} for identical conditions, we perform an Arrhenius fit (Figure 4b) to determine the activation energy. The uncertainty associated with the activation energy is quantified by the standard error of this linear fit.

Effective Order of Illumination (n): As described in the main text and in section S6 above, we first perform photoconductivity versus photon flux measurements. With the knowledge that hole activity follows a sublinear relationship with incident photon flux ($a_{h^+} \propto I_{in}^n$), we fit photoconductivity data ($\sigma_{ph} \propto I_{in}^n$) over a range of illumination intensities (0.1 to ~29 suns) and find that the relationship can accurately be described for an n value of 0.72 (rounded from 0.716). To confirm that 0.72 is an appropriate exponent to quantify the role of illumination on hole activity, we performed a model fit (Figure 4d) in which the exponent is set to be 0.72 ($r_{Pb^0} = A * I_{in}^{0.72}$ where A is the only fitting parameter). We find that we can achieve an excellent fit to the data with an r^2 of 0.97. To additionally confirm that this exponent is proper, we performed a fit (Figure S7) to a model in which both the pre-exponent and n are fitting parameters ($r_{Pb^0} = A * I_{in}^n$). Here, we see that the fit results in an n of 0.718. Thus, we take 0.72 to be the value of n. The confirmation data is comprised of runs at 125°C over a range of illumination intensities is also considered part of the 'training dataset.' All model fits are done with the curve_fit function within Python's SciPy library.

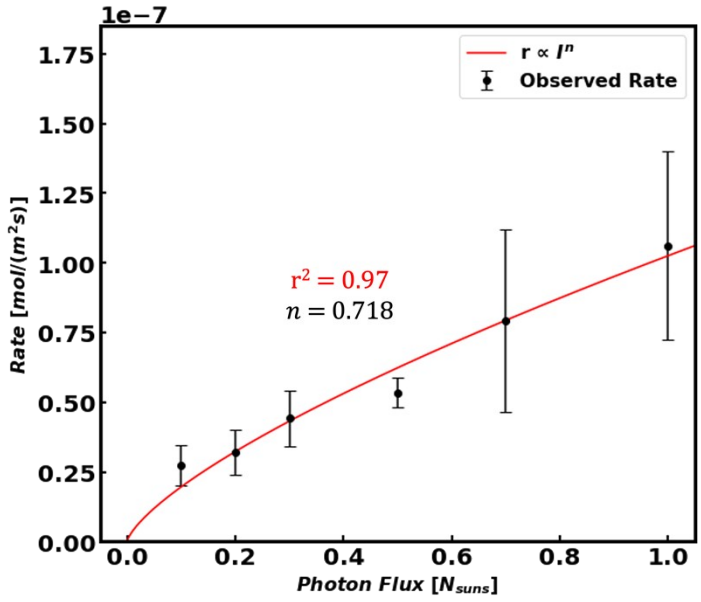

Figure S10. Fit of r_{Pb^0} with varying photon flux. Initial rate of Pb^0 formation versus photon flux (0.1-1 suns, 540 nm light) at 125°C . The exponent n is determined the be ~0.72, and r^2 of the fit is 0.97. Error bars quantify the uncertainty with the standard error of the mean for runs at identical conditions.

Preexponential Factor ($k_{0,LID}$): After setting the $E_{A,LID}^{eff}$ and n, we take the whole training dataset and calculate the preexponential that minimizes the sum of squared errors between the experimentally determined rates and the model predicted. This is a linear fitting procedure ($Observed\ rate = A \cdot \exp\left(\frac{-0.61\ eV}{k_B T}\right) * I_{in}^{0.72}$ where A is the only fit parameter). We quantify the uncertainty of this value with the standard error of the linear fit for A using the entire training dataset

8. Speculation on the Role of O_2 in Preventing Pb^0 Formation

O_2 presence in the ambient atmosphere, even in relatively small concentrations, alters the nature of the chemical reactions that the perovskite undergoes. We can visualize this by the different optical and optoelectronic progressions shown in Figures 2 and 3 in the main text. During photoexcitation, photoexcited electrons are likely to be taken up by adsorbed O_2 (O_2^*) to form superoxide radicals ($O_2^{*-\cdot}$). Thus, the chemical plausibility of a reduction reaction (i.e., Pb^{2+} reduction to Pb^0) happening is substantially less likely based on this understanding alone. While it is not possible for us to explicitly answer how O_2 prevents Pb^0 formation, we can hypothesize some plausible reactions that may occur. Principally, we want to determine what the reduced species is since it is clearly not Pb^{2+}. Note that, in many forms of halide perovskite decomposition, I_2 is the oxidized decomposition product. When O_2 is absent from the ambient atmosphere, Pb^{2+} is reduced to Pb^0. O_2 is principally altering the species that is reduced (presumably by acting as a catalyst or being consumed itself). We hypothesize two potential pathways that each begin with superoxide radical formation: (A) proton abstraction from formamidinium to produce formamidine and (B) lead-oxide formation. The two hypothetical processes begin with the adsorption of O_2 onto a surface adsorption site followed by the uptake of a conduction band electron to form a superoxide radical:

$$h\nu \rightleftharpoons e^- + h^+ \tag{1O}$$

$$O_2 + [*] \rightleftharpoons O_2^* \tag{2O}$$

$$O_2^* + e^- \rightleftharpoons O_2^{*-\cdot} \tag{3O}$$

Rather than electrons flowing from the conduction band directly to Pb^{2+} reduction, the electron path is rerouted, being taken up by adsorbed O_2 (a strong electron acceptor) and reacting instead with an organic cation or directly with Pb^{2+}. In either case, Pb^{2+} stays in its oxidized form as Pb(II) or Pb(IV).

(A) Proton abstraction from formamidinium to produce formamidine:

$$FAPbI_3 + O_2^{*-\cdot} \rightleftharpoons FA^0 + HO_2^{\cdot *} + PbI_2 + I^- \tag{1A-O}$$

$$FA^0 \rightarrow volatile\ organics\ (g\uparrow) \tag{2A-O}$$

$$HO_2^{*} \rightarrow \frac{1}{2}H_2 + O_2^{*} \quad \text{(3A-O)}$$

$$I^- + h^+ \rightarrow \frac{1}{2}I_2 \quad \text{(4A-O)}$$

with the net reaction of:

$$FAPbI_3 + h\nu \xrightarrow{O_2} FA^0 + PbI_2 + \frac{1}{2}I_2 \quad \text{(A-O)}$$

(B) Lead oxide formation:

$$FAPbI_3 + O_2^{*-\cdot} + e^- \rightarrow PbO_2 + 3I_i^- + FA_i^+ \quad \text{(1B-O)}$$

$$2I_i^- + 2h^+ \rightarrow I_2 \quad \text{(2B-O)}$$

$$I_i^- + FA_i^+ \rightarrow FAI \quad \text{(3B-O)}$$

with the net reaction of:

$$FAPbI_3 + 2h\nu + O_2 \rightarrow FAI + PbO_2 + I_2 \quad \text{(B-O)}$$

In each of the above cases, the reduced species is different than LID, but the oxidized species is still I_2. Future studies will seek to elucidate the reaction mechanisms for the photooxidation of FA-rich perovskite compositions.

9. Effect of High Temperature Exposure

Due to the relatively slow rate of this reaction coupled with the specific sensitivity of our detection instruments, we chose to fit the kinetic model with degradation experiments performed at elevated temperatures (85°C and 145°C). To determine the effects of high temperature exposure on the samples compared to high temperature with illumination, a $FA_{0.8}Cs_{0.2}Pb(I_{0.83}Br_{0.17})_3$ film was degraded in our *in-situ* degradation chamber at 145°C (maximum temperature used for rate law fitting) under 1 sun illumination from a monochromatic 540 nm green LED. Every hour for three hours, the sample was briefly removed from the flowing N_2 atmosphere to collect transmittance spectra and XRD patterns inside and outside of the degradation beam area. Figure S9 shows the results of these experiments. The changes in transmittance spectrum are very distinct between the two regions (fig. S11a,c). For the illuminated region, the transmittance decreases significantly in the low energy visible and near infrared with a slight increase at wavelengths below ~600 nm. In contrast, the transmittance spectrum outside the illuminated region changes minimally over 3 hours. In agreement with our *ex-situ* measurements shown in Figure 1, we again see the Pb^0 (111) reflection at ~31.3° as well as the $FAPbBr_3$ (001) reflection at ~14.8°. We do not observe the PbI_2 (001) peak at ~12.6° for the illuminated region but do observe a small peak associated with this reflection in the unilluminated region. The appearance of this peak is most likely attributable to thermal decomposition of formamidinium.[9] Thus, we cannot conclude that no degradation occurs because of high temperature exposure, but it is apparent that any degradation occurring is quite small in magnitude compared to LID at an identical temperature. Importantly, any degradation that may be occurring appears to minimally affect the optical properties. We have also shown that high temperatures are not required for LID Pb^0 formation in Figure 2.

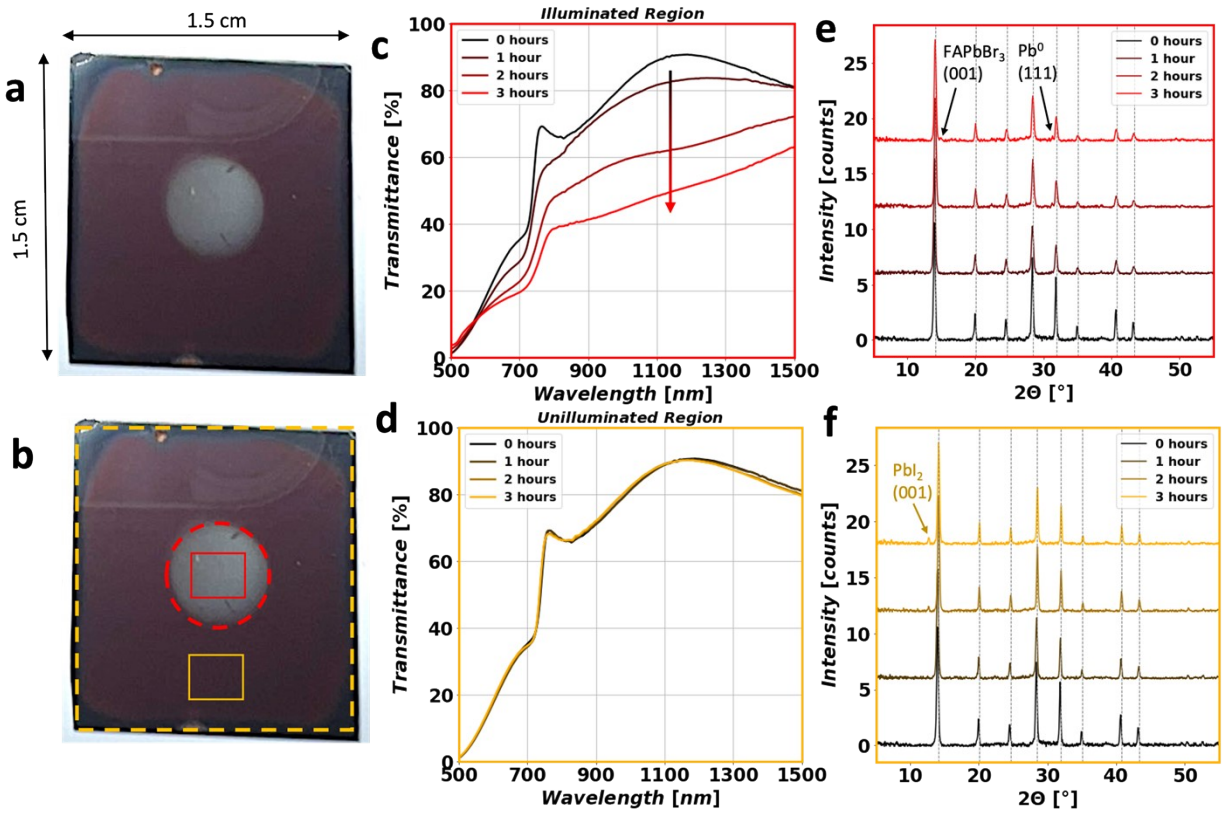

Figure S11. Effect of high temperature exposure versus high temperature exposure with illumination. *In-situ* degradation at 145°C, 1 sun green LED, flowing N_2**.** Image of the perovskite sample after 2 hours of degradation with (a) sample dimensions and (b) with reference to area illuminated by the microscope beam (red) and the unilluminated region outside the microscope beam (yellow). (c. d) Transmittance spectrum and diffraction pattern (e, f) over the course of degradation for the (c, e) illuminated region and (d, f) unilluminated region. The red and yellow rectangles in (b) are the approximate area through which the transmittance measurements were taken (as defined by a mask at the entrance of an integrating sphere); diffraction measurements are also taken inside these denoted areas (x-ray beam area defined by a 0.3 mm collimator).

10. Influence of Encapsulation on Degradation Rate

To probe how the rate of Pb^0 formation is expected to change with encapsulation (and ensuing trapping of volatile decomposition products), we encapsulated $FA_{0.8}Cs_{0.2}Pb(I_{0.83}Br_{0.17})_3$ films with a thin layer of polymethyl methacrylate (PMMA) via a spin coating procedure. PMMA precursor solution was first prepared to a concentration of 5mg/ml in chlorobenzene and subsequently spin coated onto bare perovskite samples, followed by an anneal at 100°C for 10 minutes. Encapsulation layer thickness was measured to be ~20 nm by stylus profilometry. An encapsulated and unencapsulated FACsPbIBr film were degraded side-by-side at 55°C under 1 sun illumination (broad-spectrum white LED) for 48 hours and characterized with UV-Vis-NIR absorption measurements. Here, we measure the absorptance (to avoid interference effects from the PMMA) by placing the sample in the center mount of an integrating sphere and plot the spectral absorbance as defined by the negative logarithm of one minus the absorptance. The results of this experiment are shown in Figure S11. Both encapsulated and unencapsulated films show negligible absorption in the sub bandgap region prior to degradation. After the period of degradation, the sub bandgap absorption increase is more pronounced in the unencapsulated film. This suggests that the trapping of volatile degradation products (e.g., I_2) slows the net formation of Pb^0.

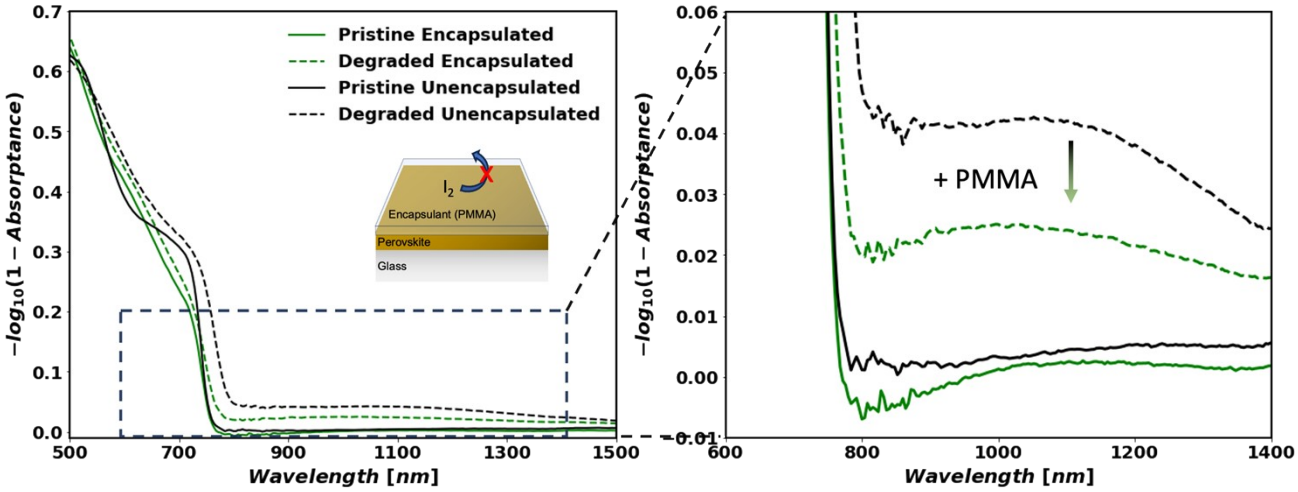

Figure S12. Light-induced degradation of $FA_{0.8}Cs_{0.2}Pb(I_{0.83}Br_{0.17})_3$ with and without encapsulation. Absorption versus wavelength for encapsulated (green) and unencapsulated (black) mixed-cation, mixed-halide films before (solid) and after (dashed) a 48-hour period of light-induced degradation. Conditions of the degradation were 55°C, 1 sun illumination from a broad-spectrum white LED.

References

(1) Braly, I. L.; Stoddard, R. J.; Rajagopal, A.; Jen, A. K. Y.; Hillhouse, H. W. Photoluminescence and Photoconductivity to Assess Maximum Open-Circuit Voltage and Carrier Transport in Hybrid Perovskites and Other Photovoltaic Materials. *Journal of Physical Chemistry Letters*. American Chemical Society July 5, 2018, pp 3779–3792. https://doi.org/10.1021/acs.jpclett.8b01152.

(2) Ross, R. T. Some Thermodynamics of Photochemical Systems. *J Chem Phys* **1967**, *46* (12), 4590–4593. https://doi.org/10.1063/1.1840606.

(3) Stoddard, R. J.; Dunlap-Shohl, W. A.; Qiao, H.; Meng, Y.; Kau, W. F.; Hillhouse, H. W. Forecasting the Decay of Hybrid Perovskite Performance Using Optical Transmittance or Reflected Dark-Field Imaging. *ACS Energy Lett* **2020**, *5* (3), 946–954. https://doi.org/10.1021/acsenergylett.0c00164.

(4) Katahara, J. K.; Hillhouse, H. W. Quasi-Fermi Level Splitting and Sub-Bandgap Absorptivity from Semiconductor Photoluminescence. *J Appl Phys* **2014**, *116* (17). https://doi.org/10.1063/1.4898346.

(5) Lu, Y.; Hu, J.; Ge, Y.; Tian, B.; Zhang, Z.; Sui, M. Decisive Influence of Amorphous PbI2−xon the Photodegradation of Halide Perovskites. *J Mater Chem A Mater* **2021**, *9* (26), 15059–15067. https://doi.org/10.1039/d1ta01730f.
(6) Siegler, T. D.; Dunlap-Shohl, W. A.; Meng, Y.; Yang, Y.; Kau, W. F.; Sunkari, P. P.; Tsai, C. E.; Armstrong, Z. J.; Chen, Y. C.; Beck, D. A. C.; Meilă, M.; Hillhouse, H. W. Water-Accelerated Photooxidation of CH3NH3PbI3Perovskite. *J Am Chem Soc* **2022**, *144* (12), 5552–5561. https://doi.org/10.1021/jacs.2c00391.
(7) Meng, Y.; Sunkari, P. P.; Meilă, M.; Hillhouse, H. W. Chemical Reaction Kinetics of the Decomposition of Low-Bandgap Tin-Lead Halide Perovskite Films and the Effect on the Ambipolar Diffusion Length. *ACS Energy Lett* **2023**, *8* (4), 1688–1696. https://doi.org/10.1021/acsenergylett.2c02733.
(8) Schellenberg, J. J. J.; Kao, K. C. C. On the Relationship between Photoconductivity and Light Intensity in Solids. *J. Phys. D: Appl. Phys* **1988**, *21*, 1764–1768.
(9) Juarez-Perez, E. J.; Ono, L. K.; Qi, Y. Thermal Degradation of Formamidinium Based Lead Halide Perovskites into: Sym -Triazine and Hydrogen Cyanide Observed by Coupled Thermogravimetry-Mass Spectrometry Analysis. *J Mater Chem A Mater* **2019**, *7* (28), 16912–16919. https://doi.org/10.1039/c9ta06058h.